Progress In Electromagnetics Research, PIER 71, 173–209, 2007

POLARIMETRIC BISTATIC SIGNATURE OF A FACETED OCTAHEDRON IN HIGH-FREQUENCY DOMAIN

G. Kubické, C. Bourlier, and J. Saillard

IREENA - EA 1770
Radar team
Ecole Polytechnique de l'Université de Nantes
Rue Christian Pauc, BP50609, 44306 Nantes Cedex 03, France

Abstract—In this paper, the bistatic polarimetric signature of a perfectly conducting faceted octahedron with high dimensions with respect to the wavelength, is considered and a closed form solution for its fast computation is developed. This particular object, composed by eight triangularly shaped trihedral corner reflectors, should exhibit a large bistatic and monostatic Radar Cross Section (RCS) over a wide angular range. Scattering from a Trihedral Corner Reflector (TCR) is dominated by single, double and triple reflections. First, shadowed areas in excitation and observation are evaluated with the help of Geometrical Optics (GO). A Physical Optics (PO) integration is performed on each plate for the computation of scattered fields, taking into account the shadowed surfaces. GO is used to take into account the lighting of each face for initial reflections of double and triple reflections. First-order diffractions, which are based on the fringe current expressions for the exterior edges of the TCR are also included in the analysis with the help of Method of Equivalent Currents / Incremental Length Diffraction Coefficients (MEC/ILDC). This permit us to calculate fast the bistatic signature of a TCR for arbitrary incidence and observation angles. The polarimetric bistatic signature of an octahedral reflector is then obtained, and results are discussed. Finally, several prospects are explained.

1. INTRODUCTION

Corner reflector is a very interesting radar target because it exhibits a large bistatic and monostatic Radar Cross Section (RCS) over a wide angular range. Indeed, this is due to double and triple reflection

contributions which provide a return of the incident wave in several directions. This justifies the employment of the TCR as radar enhancement device for navigational purposes, as appropriate reference target for RCS measurements [1, 2] and, also, for the calibration of Synthetic Aperture Radar (SAR) images [3].

The RCS is maximum when multiple internal reflections occur, that relates to the case where the transmitter and the receiver illuminate the interior region of the TCR. This configuration corresponds, in the FSA convention as shown in Fig. 1, to elevation angles $\{\pi-\theta_i;\theta_d\}$ and azimuth angles $\{\phi_i+\pi,\phi_d\}$ defined with respect to the transmitter and the receiver, respectively, and ranging from 0 to $\frac{\pi}{2}$ radians.

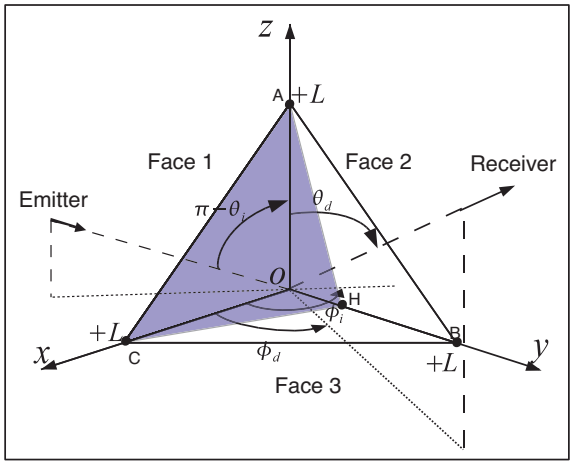

Figure 1. Illustration of the shadowed area in excitation (FSA convention).

In order to obtain a high RCS on 4π steradians, the reflector have to preserve the geometrical characteristics of the interior region of the TCR on the whole space. This reflector can be obtained by assembling eight TCRs with isosceles right triangular faces mutually orthogonal which correspond to faceted trirectangular tetrahedrons. This Octahedral Reflector (OR), which is rigorously a faceted octahedron, is depicted in Fig. 2. The trihedral corners are assumed to be perfectly conducting, so they are considered all independent, that is to say, there is any coupling effect between all the trihedral corner reflectors.

Consequently, the signature of the octahedral reflector can be obtained from the coherent summation of the signature of each trihedral corner reflector all expressed in the same system of

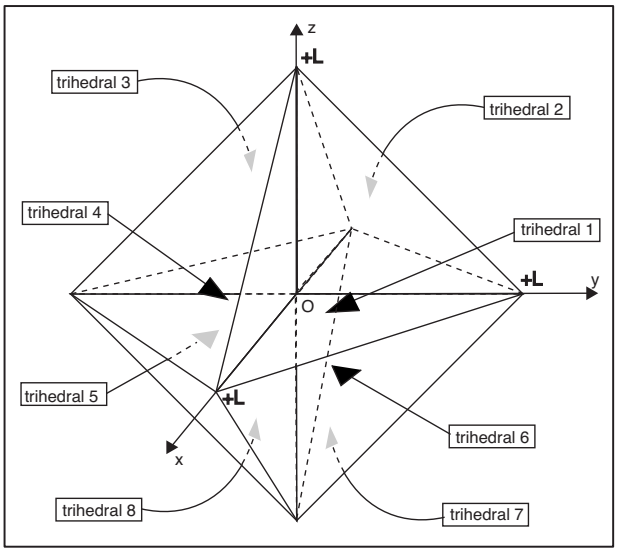

Figure 2. The octahedral reflector.

coordinates. However, many TCRs in the OR can be illuminated and/or observed laterally, so the bistatic signature of the TCR must be evaluated for any excitation and observation angles.

By using high-frequency methods, the bistatic signature of the octahedral reflector has never been evaluated, until now. In this paper, this calculus is detailed and obtained from the bistatic signature of the TCR on 4π steradians.

This method is based on the works of Corona et al. [4] and Polycarpou et al. [5] but with a different formalism using properties of the Sinclair matrix and some matrix relations [6, 7]. Corona et al. and Polycarpou et al. used a similar approach in order to evaluate the monostatic RCS of the TCR but those works were all done in the restricted domain of the interior region of the TCR and with a formalism which is not really appropriate for the more general context of our work. So, the calculus proposed here is a generalization, with an appropriate formalism (Sinclair matrix), to the bistatic full-polarimetric case and for any excitation and observation angles. This means that the TCR can be illuminated and observed laterally inducing shadowed regions in excitation [8], as shown in Fig. 1, and in observation, Fig. 3.

Results in co and cross-polarisation, in monostatic and bistatic case, will be compared to a numerical method (Multi-Level Fast Multipole Method as explained in [9, 10]).

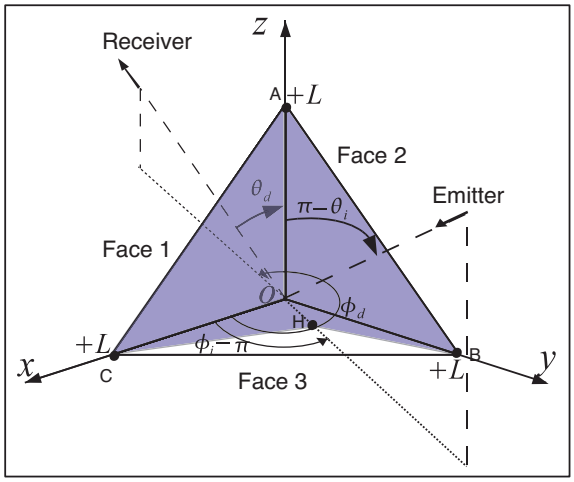

Figure 3. Illustration of the shadowed area in observation (FSA convention).

2. APPROACH

Corona et al. and Polycarpou et al. [4, 5] have shown that the first order edge diffractions and the single, double and triple reflections are the principal contributions in the signature of the TCR.

PO and GO are used for the calculation of single, double and triple reflections from the corner reflector plates, whereas the Method of Equivalent Currents (MEC) [11–14] is used for the calculation of the first-order diffractions from the exterior edges. PO approximation is applied on each face to evaluate the single reflection contribution. For double and triple reflections, the GO approximation is used for the calculation of the initial reflected fields and the PO is then applied only for the last reflection. To obtain a signature valid for any excitation and observation angles, the shadowing effect is taken into account with the help of GO. Thus, the shadowed surfaces are used to evaluate the area, which are both illuminated and observed, on which PO is finally applied.

As well known, Geometrical Optics (GO) assumes that an electromagnetic plane wave impinging on a plane whose dimensions are much greater than the incident wavelength (high-frequency region) will still be reflected in the specular direction as a plane wave. It is an asymptotic expansion of the scattered field in the far field. In this way, diffraction effects caused by the finite nature of the scatterer are completely neglected. Thus, the PO theory improves the GO

results by taking into account the diffraction effects. Indeed, The PO approximation is an asymptotic expansion of the induced current on the surface of the target. This is an integral approach based on the assumption that the induced currents on the surface of the scatterer are known. When the scatterer is a perfectly conducting body, the approximated expressions of the surface currents are assumed to be:

$$\vec{J}_{po}(\vec{r}) = 2\hat{n}(\vec{r}) \wedge \vec{H}_i(\vec{r}) \tag{1}$$

$$\vec{M}_{po}(\vec{r}) = \vec{0} \tag{2}$$

$\vec{H}_i(\vec{r})$ is the incident magnetic field on the surface and $\hat{n}$ is the normal to the surface. The PO surface current density is integrated over the illuminated and observed area of the plate. For the single reflection case, the observed surface of each illuminated region is evaluated by taking into account the shadowed region in excitation and observation. In general case, after evaluating the existence of each double and triple reflections that could occur, the both illuminated and observed surfaces are evaluated by taking into account the shadowed regions in excitation on the first plates of the reflections, and the shadowed regions in observation on the last plates of the reflections. For double and triple reflections, the GO approximation is used in order to evaluate finally the illuminated region on the last plate for the calculation of the scattered field on this face.

For instance, from Fig. 1 and Fig. 3, according to the laws of geometrical optics, for arbitrary angles of incidence and observation, there may be shadowed regions. In Fig. 1, the triangular face (AOC) is excited on the backside, it induces a shadowed region on the two others faces. The illuminated patches are finally (BHC) and (BHA) for the single reflection components. Double reflection needs the use of GO to evaluate the illuminated area which does not appear on the draw. In Fig. 3, only a part of the triangular face (BOC) is visible due to the shadowing effect in observation.

In this paper, we assume time dependence $e^{+j\omega t}$.

3. SIGNATURE OF THE OCTAHEDRAL REFLECTOR

The bistatic signature of an octahedral reflector is obtained from the coherent summation of the signature of each TCR, all expressed in the global system of coordinates associated to the octahedral reflector:

$$\left[S^{OR}\right] = \sum_{k=1}^{8} \left[S_{global}^{TCR_k}\right] \tag{3}$$

The bistatic signature of a TCR, in the global system of coordinates $(0, x, y, z)$, is derived from the signature of the TCR obtained in its own local system of coordinates $(0, x_k, y_k, z_k)$, with the help of the matrix $[P]$ defined as follows:

$$[P(\theta,\phi;\alpha_{e_k},\beta_{e_k},\gamma_{e_k};\theta_k,\phi_k)] = [R_s(\theta,\phi)]^T\,[R_e(\alpha_{e_k},\beta_{e_k},\gamma_{e_k})]\,[R_s(\theta_k,\phi_k)] \tag{4}$$

The symbol T stands for the matrix transpose and k represents the number of the considered TCR: $k = \{1 \text{ to } 8\}$.

- $[R_s(\theta,\phi)]$ is the spheric rotation matrix which gives the relation between a Cartesian basis ($\vec{u}_x$, $\vec{u}_y$, $\vec{u}_z$) and a spherical basis ($\vec{u}_r$, $\vec{u}_\theta$, $\vec{u}_\phi$). (θ,ϕ) are the azimuth and elevation angles, defined in FSA convention for the incident wave and diffracted wave as in Fig. 1.
- $\left[R_e(\alpha_{e_{j_1}},\beta_{e_{j_1}},\gamma_{e_{j_1}})\right]$ is the Euler rotation matrix which gives the transformation from the global system of coordinates (O, x, y, z) to the local system of coordinates (O,x_k,y_k,z_k) with the help of three rotations of angles α_{e_k}, β_{e_k} and γ_{e_k}.
- $[R_s(\theta_k,\phi_k)]$ is the spheric rotation matrix which gives the relation between a Cartesian basis ($\vec{u}_{x_k}$, $\vec{u}_{y_k}$, $\vec{u}_{z_k}$) and a spherical basis ($\vec{u}_{r_k}$, $\vec{u}_{\theta_k}$, $\vec{u}_{\phi_k}$)

The Euler rotation matrix is defined as follows:

$$\begin{aligned}
[Re_k(\alpha_{e_k},\beta_{e_k},\gamma_{e_k})] &= \begin{bmatrix} Re_{k_{11}} & Re_{k_{12}} & Re_{k_{13}} \\ Re_{k_{21}} & Re_{k_{22}} & Re_{k_{23}} \\ Re_{k_{31}} & Re_{k_{32}} & Re_{k_{33}} \end{bmatrix} \\
&= \begin{bmatrix} c(\alpha_{e_k})c(\gamma_{e_k}) - s(\alpha_{e_k})c(\beta_{e_k})s(\gamma_{e_k}) \\ s(\alpha_{e_k})c(\gamma_{e_k}) + c(\alpha_{e_k})c(\beta_{e_k})s(\gamma_{e_k}) \\ s(\beta_{e_k})s(\gamma_{e_k}) \end{bmatrix} \\
&\quad \begin{matrix} -c(\alpha_{e_k})s(\gamma_{e_k}) - s(\alpha_{e_k})c(\beta_{e_k})c(\gamma_{e_k}) & s(\alpha_{e_k})s(\beta_{e_k}) \\ -s(\alpha_{e_k})s(\gamma_{e_k}) + c(\alpha_{e_k})c(\beta_{e_k})c(\gamma_{e_k}) & -c(\alpha_{e_k})s(\beta_{e_k}) \\ s(\beta_{e_k})c(\gamma_{e_k}) & c(\beta_{e_k}) \end{matrix} \end{bmatrix}
\end{aligned} \tag{5}$$

With $c(x) = \cos(x)$ and $s(x) = \sin(x)$. With the rotation angles defined as:

$$\alpha_{e_k} = \frac{\pi}{2}(k-1) \tag{6}$$

$$\gamma_{e_k} = 0 \tag{7}$$

$$\beta_{e_k} = \left\lfloor \frac{k-1}{4} \right\rfloor \pi \tag{8}$$

For $k = \{1 \text{ to } 8\}$. With the floor function: $\lfloor x \rfloor = \sup\{n \in Z \mid n \leq x\}$

These rotation angles allow to obtain the vectors of the basis of each local system of coordinates associated to the TCR:

$$\vec{u}_{x_k} = \begin{bmatrix} Re_{k_{11}} \\ Re_{k_{21}} \\ Re_{k_{31}} \end{bmatrix} \qquad \vec{u}_{y_k} = \begin{bmatrix} Re_{k_{12}} \\ Re_{k_{22}} \\ Re_{k_{32}} \end{bmatrix} \qquad \vec{u}_{z_k} = \begin{bmatrix} Re_{k_{13}} \\ Re_{k_{23}} \\ Re_{k_{33}} \end{bmatrix} \tag{9}$$

The spheric rotation matrix is defined as follows:

$$[R_s(\theta,\phi)] = \begin{bmatrix} \sin(\theta)\cos(\phi) & \cos(\theta)\cos(\phi) & -\sin(\phi) \\ \sin(\theta)\sin(\phi) & \cos(\theta)\sin(\phi) & \cos(\phi) \\ \cos(\theta) & -\sin(\theta) & 0 \end{bmatrix} \tag{10}$$

Thus, the matrix $[P]$ allows the transition between the spherical components of the field expressed in the spherical basis $(\vec{u}_r,\ \vec{u}_\theta,\ \vec{u}_\phi)$ defined in the global system of coordinates (O,x,y,z) with the angles (θ,ϕ), and the spherical components expressed in the spherical basis $(\vec{u}_{r_k},\ \vec{u}_{\theta_k},\ \vec{u}_{\phi_k})$ defined in the local system of coordinates (O,x_k,y_k,z_k) with the angles (θ_k,ϕ_k). The signature of the TCR expressed in its own local system of coordinates is then evaluated in the global system of coordinates:

$$\begin{bmatrix} 0 & 0 & 0 \\ 0 & \left[S^{TCR_k}_{global}\right] \\ 0 & \end{bmatrix} = [P_{dk}] \begin{bmatrix} 0 & 0 & 0 \\ 0 & \left[S^{TCR_k}_{local-k}\right] \\ 0 & \end{bmatrix} [P_{ik}]^T \tag{11}$$

With:

$$[P_{dk}] = [R_s(\theta_d,\phi_d)]^T [R_e(\alpha_{e_k},\beta_{e_k},\gamma_{e_k})] [R_s(\theta_{d_k},\phi_{d_k})] \tag{12}$$

$$[P_{ik}] = [R_s(\theta_i,\phi_i)]^T [R_e(\alpha_{e_k},\beta_{e_k},\gamma_{e_k})] [R_s(\theta_{i_k},\phi_{i_k})] \tag{13}$$

The local spheric angles are obtained with:

$$\theta_{p_k} = \arccos\left(\vec{u}^{\,p}_r \cdot \vec{u}_{z_k}\right) \tag{14}$$

$$\phi_{p_k} = \arctan\left(\frac{\vec{u}^{\,p}_r \cdot \vec{u}_{y_k}}{\vec{u}^{\,p}_r \cdot \vec{u}_{x_k}}\right) \tag{15}$$

With $\theta_{p_k} \in [0;\pi]$ and $\phi_{p_k} \in [0;2\pi]$ for $p = i$ or d.

The bistatic signature of the TCR k, expressed in its own local system of coordinates is calculated by the coherent summation of all the contributions occurring for the TCR k, all expressed in the local system of coordinates associated to the TCR k:

$$\left[S^{TCR_k}_{local-k}\right] = \left[S^{sd}_k\right] + [S^{sr}_k] + \left[S^{dr}_k\right] + \left[S^{tr}_k\right] \tag{16}$$

Where

- $\left[S_k^{sd}\right]$ is the bistatic signature of the first order edge-diffraction contribution, also named single diffraction, of the exterior edges of the TCR, expressed in the local system of coordinates of the TCR k.
- $[S_k^{sr}]$ is the bistatic signature of the single reflection contribution expressed in the local system of coordinates of the TCR k.
- $\left[S_k^{dr}\right]$ is the bistatic signature of the double reflection contribution expressed in the local system of coordinates of the TCR k.
- $[S_k^{tr}]$ is the bistatic signature of the triple reflection contribution expressed in the local system of coordinates of the TCR k.

The single reflection on the exterior of the trihedral corner (single reflection for faces illuminated on the backside) is not taken into account in the signature of the TCR because for the octahedral reflector, these contributions correspond to single internal reflection of other TCRs.

The next parts of this paper present the evaluation of all of these contributions. Calculations are done in the local system of coordinates of the trihedral reflector numbered k. In the following, the local system of coordinates (O,x_k,y_k,z_k) is considered as the global system of coordinates, in order to improve the comprehension.

4. SINGLE REFLECTION OF THE TRIHEDRAL CORNER REFLECTOR

The procedure of the calculus is the same for the three faces, so we use a label "j_1" with $j_1 = \{1, 2, 3\}$. In fact j_1 represents the number of the face on which the single reflection is evaluated. The faces are numbered as shown in Fig. 1. So, the contribution is calculated for the three faces in their local system of coordinates. The existence of each reflection is evaluated by two conditions:

$$\vec{u}_r^{\,i} \cdot \vec{u}_{z_{j_1}} < 0 \tag{17}$$

$$\vec{u}_r^{\,d} \cdot \vec{u}_{z_{j_1}} > 0 \tag{18}$$

The face j_1 is excited by the incident wave if the first condition is validated, and if the second one is validated the face is observed by the receiver. So the single reflection calculation can be done for the face j_1. The faces of the TCR are defined from Fig. 4, and the local cartesian basis system, defined in the global system of coordinates associated to

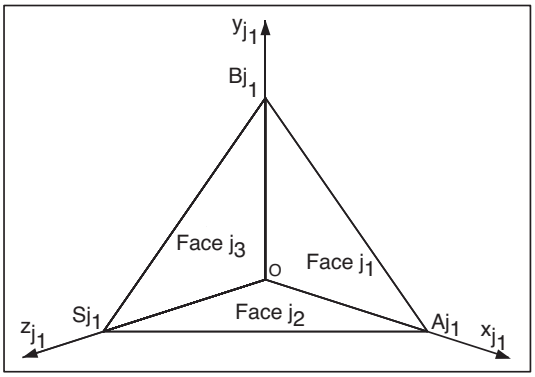

Figure 4. Configuration for the single reflection calculus.

the trihedral corner is:

$$\vec{u}_{x_{j_1}} = \begin{bmatrix} \delta^3_{j_1} \\ \delta^2_{j_1} \\ \delta^1_{j_1} \end{bmatrix} \quad \vec{u}_{y_{j_1}} = \begin{bmatrix} \delta^1_{j_1} \\ \delta^3_{j_1} \\ \delta^2_{j_1} \end{bmatrix} \quad \vec{u}_{z_{j_1}} = \begin{bmatrix} \delta^2_{j_1} \\ \delta^1_{j_1} \\ \delta^3_{j_1} \end{bmatrix} \tag{19}$$

$$j_1 = \{1, 2, 3\}$$

And where δ^j_i is the Kronecker delta:

$$\delta^j_i = \begin{cases} 1 & \text{if} \quad i = j \\ 0 & \text{if} \quad i \neq j \end{cases} \tag{20}$$

The calculus is made in the local system of coordinates of the face j_1, i.e: $(O_{j_1}, x_{j_1}, y_{j_1}, z_{j_1})$, in order to generalise the method for the three faces. We set the three vertices of the trihedral corner defined in the local system of coordinates $(O_{j_1}, x_{j_1}, y_{j_1}, z_{j_1})$:

$$A_{j_1} = \begin{bmatrix} +L \\ 0 \\ 0 \end{bmatrix} B_{j_1} = \begin{bmatrix} 0 \\ +L \\ 0 \end{bmatrix} S_{j_1} = \begin{bmatrix} 0 \\ 0 \\ +L \end{bmatrix} \tag{21}$$

We also define the two other faces j_2 and j_3 such as the faces j_1, j_2 and j_3 are numbered in the direct sense, this an arbitrary choice but this must be defined for the following, so:

$$\begin{aligned} j_1 &= \{1, 2, 3\} \\ j_2 &= \text{Mod}(j_1, 3) + 1 \\ j_3 &= 6 - j_1 - j_2 \end{aligned}$$

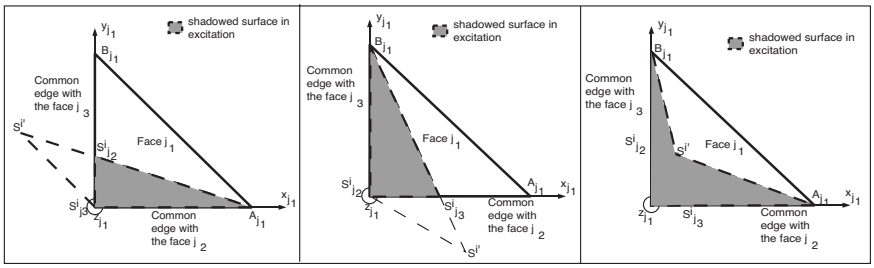

Figure 5. Shadowing effect in incidence on the face j_1 for the single reflection calculus.

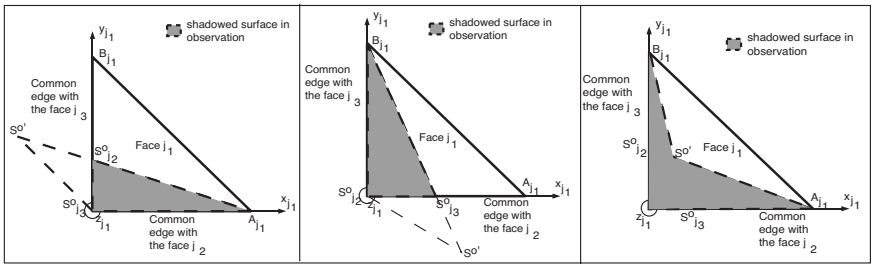

Figure 6. Shadowing effect in observation on the face j_1 for the single reflection calculus.

Where the modulo operation $\mathrm{Mod}(x, y)$ finds the remainder of division of x by y

The problem geometry is illustrated in Fig. 4. First, we determine the point $S^{i'}$ by doing a projection in the excitation direction, of the vertex S_{j_1} on the considered plate called j_1. In Fig. 5, the three possibilities of shadowing effect in excitation are depicted. The same way is used to obtain the point $S^{o'}$ defined with respect to the observation. In Fig. 6 the three possibilities of shadowing effect in observation are depicted. By knowing the coordinates of $S^{i'}$ and $S^{o'}$, one can evaluate the shadowed regions in excitation and observation by calculating intersection with the limits of the face. By taking into account the intersection of these shadowed regions, the both illuminated and observed patch is finally evaluated. The shape of the surface used for the calculation is an arbitrary triangle shown in Fig. 7.

The signature of the single reflection of the considered plate is then derived from the local signature of elementary triangle from the PO theory given in Appendix A, and expressed in the local system of coordinates of the plate j_1.

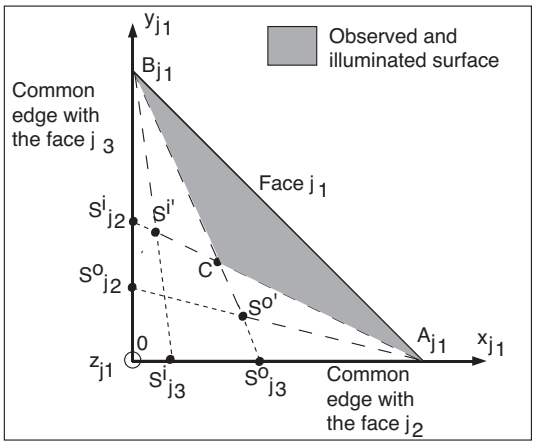

Figure 7. Example of shadowing effect in incidence and observation for the single reflection contribution.

The signature of the single reflection expressed in the local system of coordinates of the plate j_1 is then evaluated in the global system of coordinates associated to the TCR k:

$$\begin{bmatrix} 0 & 0 & 0 \\ 0 & \left[S^{sr}_{j_1 global-k}\right] & \\ 0 & & \end{bmatrix} = [P_{dj_1}] \begin{bmatrix} 0 & 0 & 0 \\ 0 & \left[S^{sr}_{j_1 local-j_1}\right] & \\ 0 & & \end{bmatrix} [P_{ij_1}]^T \tag{22}$$

The matrices $[P_{dj_1}]$ and $[P_{ij_1}]$ are defined from Eqs. (4), (12) and (13).

Signature of single reflection contribution expressed in the global system of coordinates of the trihedral reflector k is the summation of the signature of the single reflection of each face evaluated in this global system of coordinates:

$$[S^{sr}_k] = \sum_{j_1=1}^{3} \left[S^{sr}_{j_1 global-k}\right] \tag{23}$$

The next section presents the evaluation of the double reflection contribution.

5. DOUBLE REFLECTION OF THE TRIHEDRAL CORNER REFLECTOR

There are six double reflections, three in the direct sense: $1 \to 2$, $2 \to 3$, $3 \to 1$, and three others in the indirect sense: $1 \to 3$, $2 \to 1$, $3 \to 2$.

The procedure of the calculus is the same for all the double reflections, so we use the label "j_1" with $j_1 = \{1, 2, 3\}$. In fact j_1 represents the number of the first face on which the first reflection occurs. The double reflection considered is $j_1 \rightarrow j_2$. The GO approximation permits to calculate the characteristics of the reflected ray on the first face of the double reflection. The specular reflection direction is defined, in the local system of coordinates associated to the face j_1, by the spherical angles $(\theta_{r_{j_1 j_2}}, \phi_{r_{j_1 j_2}})$ obtained from the spherical angles of incidence $(\theta_{i_{j_1}}, \phi_{i_{j_1}})$ evaluated from Eqs. (14) and (15):

$$\theta_{r_{j_1 j_2}} = \pi - \theta_{i_{j_1}} \tag{24}$$

$$\phi_{r_{j_1 j_2}} = \phi_{i_{j_1}} \tag{25}$$

Moreover, $\vec{u}_{z_{j_1}}$ is a normal unit vector of the face j_1, so the reflection director vector of the reflected ray on the face j_1 towards a face j_2 is evaluated in the global system of coordinates of the TCR k:

$$\vec{u}_r^{\,r j_1 j_2} = \vec{u}_r^{\,i} - 2(\vec{u}_r^{\,i} \cdot \vec{u}_{z_{j_1}})\vec{u}_{z_{j_1}} \tag{26}$$

And finally

$$\vec{u}_r^{\,r j_1 j_2} = \begin{bmatrix} (1 - 2\delta_{j_1}^2)\sin(\theta_i)\cos(\phi_i) \\ (1 - 2\delta_{j_1}^1)\sin(\theta_i)\sin(\phi_i) \\ (1 - 2\delta_{j_1}^3)\cos(\theta_i) \end{bmatrix} \tag{27}$$

The ray reflected on the face j_1 can encounter the two other faces of the trihedral reflector. Faces being numbered, double reflections in the direct sense ($1 \rightarrow 2$, $2 \rightarrow 3$, $3 \rightarrow 1$) and in the indirect sense ($1 \rightarrow 3$, $2 \rightarrow 1$, $3 \rightarrow 2$) are distinguished. The subscript of the second face of the double reflection j_2 is defined as:

$$j_2 = j_{2_i}(1 - \text{sense})/2 + j_{2_d}(1 + \text{sense})/2 \tag{28}$$

With

$$\begin{gathered} \text{sense} = +1; -1 \\ j_{2_d} = \text{Mod}(j_1, 3) + 1 \\ j_{2_i} = 6 - j_1 - j_{2_d} \end{gathered}$$

So, the third face which participates in the double reflection only for the shadowing effect is:

$$j_3 = 6 - j_1 - j_2 \tag{29}$$

The second reflection on the face j_2 occurs only if the director vector of the reflected ray by the face j_1 satisfies the relation:

$$\vec{u}_r^{\,r j_1 j_2} \cdot \vec{u}_{z_{j_2}} \leq 0 \tag{30}$$

$\vec{u}_{z_{j_2}}$ is the normal unit vector of the face j_2. Eq. (30) ensures that the reflected wave (after the first reflection) will encounter the face j_2, and implies that the face j_2 does not create a shadowing effect in excitation on the face j_1. So, the double reflection must be evaluated for only two cases: shadowing effect in excitation due to the face j_3 on the face j_1 and the case for no shadowing effect in excitation.
So, the existence of each double reflection is evaluated by three conditions:

$$\vec{u}_r^i \cdot \vec{u}_{z_{j_1}} < 0 \tag{31}$$

$$\vec{u}_r^i \cdot \vec{u}_{z_{j_2}} < 0 \tag{32}$$

$$\vec{u}_r^d \cdot \vec{u}_{z_{j_2}} > 0 \tag{33}$$

The face j_1 is excited by the incident wave if the first condition (31) is validated. If the second (33) holds, the face j_2 does not shadow the face j_1 in excitation. Finally, if the third one (32) is satisfied the face j_2 is observed by the receiver. So the double reflection $j_1 \rightarrow j_2$ must be calculated.

As the single reflection, the shadowed region in excitation is evaluated on the first plate of the double reflection, by geometrical projection parallel to the direction of incidence. Then, the illuminated surface on the face j_1 can be projected on the face j_2 parallel to the specular reflection direction.

The director vector of the reflected ray can be easily evaluated in the local system of coordinates of the face j_2:

$$\vec{u}_i^{j_2} = \begin{bmatrix} \sin(\theta_{i_{j_2}})\cos(\phi_{i_{j_2}}) \\ \sin(\theta_{i_{j_2}})\sin(\phi_{i_{j_2}}) \\ \cos(\theta_{i_{j_2}}) \end{bmatrix} \tag{34}$$

$(\theta_{i_{j_2}}, \phi_{i_{j_2}})$ are the spherical angles of incidence in the local system of coordinates of the face j_2 obtained from the director vector of the reflected ray and from Eqs. (14) and (15):

$$\theta_{i_{j_2}} = \arccos\left(\vec{u}_r^{rj_1j_2} \cdot \vec{u}_{z_{j_2}}\right) \tag{35}$$

$$\phi_{i_{j_2}} = \arctan\left(\frac{\vec{u}_r^{rj_1j_2} \cdot \vec{u}_{y_{j_2}}}{\vec{u}_r^{rj_1j_2} \cdot \vec{u}_{x_{j_2}}}\right) \tag{36}$$

With $\theta_{i_{j_2}} \in [0;\pi]$ and $\phi_{i_{j_2}} \in [0;2\pi]$.

With the help of $\vec{u}_i^{j_2}$, the illuminated surface on the face j_2 is obtained by geometrical projection of the illuminated surface of the

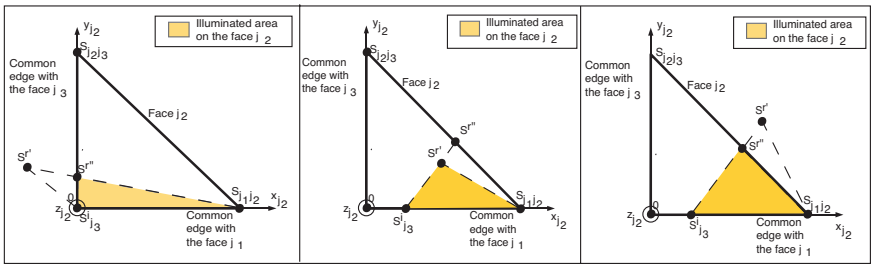

Figure 8. Illuminated surface on the face j_2 after the first reflection during double reflection in the indirect sense case.

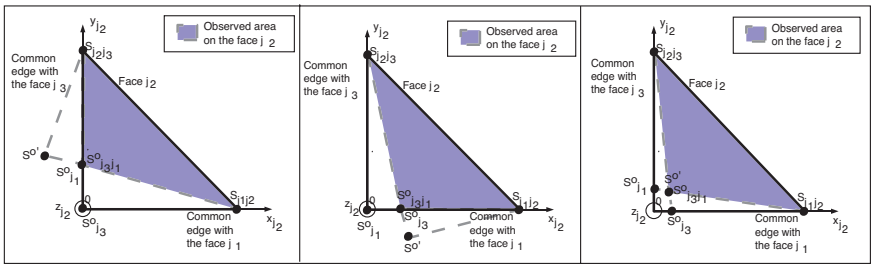

Figure 9. Shadowing effect in observation on the face j_2 for the double reflection calculus in the indirect sense case.

face j_1 on the face j_2. Three cases can be obtained for a given sense, they are depicted in Fig. 8 for the case of an indirect sense of double reflection.

However, there are four possibilities for the observation during the second reflection occurring on j_2: shadowing effect in observation by the face j_1 on j_2, shadowing effect in observation by the face j_3 on j_2, shadowing effect in observation by the faces j_1 and j_3 on j_2, no shadowing effect in observation. As in the single reflection case, the shadowed surfaces in observation can be obtain by geometrical projection parallel to the observation direction. The three cases obtained are depicted in Fig. 9 for the case of an indirect sense of double reflection. Six configurations of combination of illuminated surfaces and observed surfaces are encountered Figs. 10 and 11 for the case of an indirect sense of double reflection.

From appropriate tests and calculus of intersection, the both illuminated and observed surface is evaluated. It can be an arbitrary triangle or an arbitrary quadrilateral. These tests and calculus can be easily generalise for the two senses of double reflection. The signature

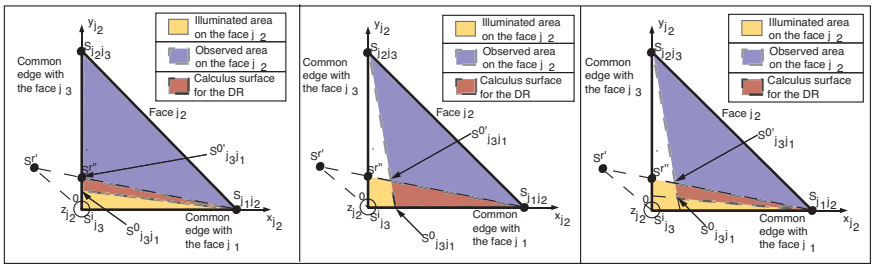

Figure 10. Intersections of illuminated and observed surfaces on the face j_2 for the double reflection calculus in the indirect sense case: no shadowing effect in excitation on the face j_1.

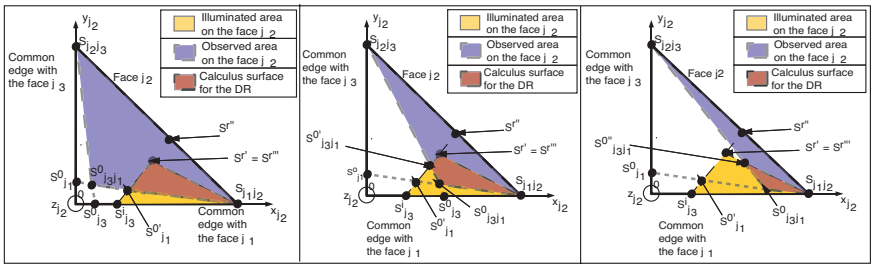

Figure 11. Intersections of illuminated and observed surfaces on the face j_2 for the double reflection calculus in the indirect sense case: shadowing effect in excitation on the face j_1.

of the double reflection $j_1 \rightarrow j_2$ is then derived from the signature of elementary triangle from the PO theory (appendix A) expressed in the local system of coordinates of the plate j_2. If the surface is a quadrilateral, it can be broken up into two elementary triangles, and the signature is obtained by the coherent summation of the two signatures of the elementary and independent triangles.
The signature of the double reflection expressed in the local system of coordinates of the plate j_2 is then evaluated in the global system of coordinates associated to the TCR k:

$$\begin{bmatrix} 0 & 0 & 0 \\ 0 & \left[S^{dr}_{j_1 j_2\ global-k}\right] & \end{bmatrix} = \left[P_{d_{j_2}}\right] \begin{bmatrix} 0 & 0 & 0 \\ 0 & \left[S^{dr}_{j_1 j_2\ local-j_2}\right] & \end{bmatrix} \times [P_{j_2 j_1}]\ [F]\ \left[P_{i_{j_1}}\right]^T \tag{37}$$

The reflection on the first face j_1 of the double reflection is treated by the GO approximation. The specular direction is used for the

geometrical projection, as seen before, and the Fresnel coefficients are applied with the help of the matrix $[F]$, composed by the Fresnel coefficients for the perfectly conducting case:

$$[F] = \begin{bmatrix} 0 & 0 & 0 \\ 0 & 1 & 0 \\ 0 & 0 & -1 \end{bmatrix} \tag{38}$$

The matrices $[P_{dj_2}]$ and $[P_{ij_1}]$ are defined with the help of Eqs. (4), (12) and (13) using appropriate subscripts. $[P_{j_2j_1}]$ is defined as:

$$\begin{aligned}[P_{j_2j_1}] = & \left[R_s(\theta_{i_{j_2}}, \phi_{i_{j_2}})\right]^T \left[R_e(\alpha_{e_{j_2}}, \beta_{e_{j_2}}, \gamma_{e_{j_2}})\right]^T \\ & \times \left[R_e(\alpha_{e_{j_1}}, \beta_{e_{j_1}}, \gamma_{e_{j_1}})\right] \left[R_s(\theta_{r_{j_1j_2}}, \phi_{r_{j_1j_2}})\right]\end{aligned} \tag{39}$$

Signature of double reflection contribution expressed in the global system of coordinates of the trihedral reflector k is the summation of the signature of each double reflection, that could occur, evaluated in this global system of coordinates:

$$\left[S_k^{dr}\right] = \sum_{j_1=1}^{3} \sum_{j_2=1}^{3} \left[S_{j_1j_2\ global-k}^{dr}\right] \quad \text{with} \quad j_1 \neq j_2 \tag{40}$$

After evaluating the double reflection contribution, now let us focus on the calculation of the triple reflection contribution.

6. TRIPLE REFLECTION OF THE TRIHEDRAL CORNER REFLECTOR

There are six triple reflections, three in the direct sense: $(1 \to 2 \to 3)$, $(2 \to 3 \to 1)$, $(3 \to 1 \to 2)$, and three others in the indirect sense: $(1 \to 3 \to 2)$, $(2 \to 1 \to 3)$, $(3 \to 2 \to 1)$.

The reflexion on the first face was detailed in the above section. The same method is applied to study the reflection on the second face during the triple reflection.

The ray reflected on the face j_2 can encounter the two other faces of the trihedral reflector. Faces being numbered, triple reflections in the direct sense and in the indirect sense are distinguished. The numbering of the subscripts of the faces are used to generalise the calculus for each triple reflection, they have been already given in the previous section. So, the triple reflection considered is $j_1 \to j_2 \to j_3$. The specular reflection direction of the second reflection is defined, in the local system of coordinates associated to the face j_2, by the spherical

angles $(\theta_{r_{j_2j_3}}, \phi_{r_{j_2j_3}})$ obtained from the spherical angles of incidence $(\theta_{i_{j_2}}, \phi_{i_{j_2}})$ obtained in the previous section:

$$\theta_{r_{j_2j_3}} = \pi - \theta_{i_{j_2}} \tag{41}$$

$$\phi_{r_{j_2j_3}} = \phi_{i_{j_2}} \tag{42}$$

Moreover, $\vec{u}_{z_{j_2}}$ is a normal unit vector of the face j_2, so the reflection director vector of the reflected ray on the face j_2 towards the face j_3 is evaluated in the global system of coordinates of the TCR k:

$$\vec{u}_r^{rj_2j_3} = \vec{u}_r^{rj_1j_2} - 2(\vec{u}_r^{rj_1j_2} \cdot \vec{u}_{z_{j_2}})\vec{u}_{z_{j_2}} \tag{43}$$

And finally, after vectorial operations:

$$\vec{u}_r^{rj_2j_3} = \begin{bmatrix} (1-2\delta_{j_1}^2)(1-2\delta_{j_2}^3)\sin(\theta_i)\cos(\phi_i) \\ (1-2\delta_{j_1}^1)(1-2\delta_{j_2}^1)\sin(\theta_i)\sin(\phi_i) \\ (1-2\delta_{j_1}^3)(1-2\delta_{j_2}^3)\cos(\theta_i) \end{bmatrix} \tag{44}$$

The third reflection on the face j_3 occurs only if the director vector of the reflected ray by the face j_2 respects the relation:

$$\vec{u}_r^{rj_2j_3} \cdot \vec{u}_{z_{j_3}} \leq 0 \tag{45}$$

$\vec{u}_{z_{j_3}}$ is the normal unit vector of the face j_3. Eq. (45) ensures that the reflected wave (after the first and second reflection) will encounter the face j_3, and implies that the face j_2 and j_3 do not create a shadowing effect in excitation on the face j_1. So, the triple reflection must be evaluated only for the case where there is no shadowing effect in excitation.

So, the existence of each triple reflection is evaluated by four conditions:

$$\vec{u}_r^i \cdot \vec{u}_{z_{j_1}} < 0 \tag{46}$$

$$\vec{u}_r^i \cdot \vec{u}_{z_{j_2}} < 0 \tag{47}$$

$$\vec{u}_r^i \cdot \vec{u}_{z_{j_3}} < 0 \tag{48}$$

$$\vec{u}_r^d \cdot \vec{u}_{z_{j_3}} > 0 \tag{49}$$

The face j_1 is excited by the incident wave if the first condition (46) is satisfied, if the second (47) and third ones (48) hold, the faces j_2 and j_3 do not shadow the face j_1 in excitation. Finally, if the fourth one (49) is validated the face j_3 is observed by the receiver. So the triple reflection $j_1 \rightarrow j_2 \rightarrow j_3$ must be calculated.

As the single and double reflection, the illuminated surface on the face j_1 is projected on the face j_2 parallel to the specular reflection direction. But, the shadowing effect can not occur in excitation, so the illuminated surface on j_1 is the total surface of the face. This configuration of illuminated surface on the face j_2 corresponds to the case depicted on the left in Fig. 8.

The director vector of the reflected ray, for the second reflection of the triple reflection, can be easily evaluated in the local system of coordinates of the face j_3:

$$\vec{u}_i^{j_3} = \begin{bmatrix} \sin(\theta_{i_{j_3}})\cos(\phi_{i_{j_3}}) \\ \sin(\theta_{i_{j_3}})\sin(\phi_{i_{j_3}}) \\ \cos(\theta_{i_{j_3}}) \end{bmatrix} \tag{50}$$

$(\theta_i^{j_3}, \phi_i^{j_3})$ are the spherical angles of incidence in the local system of coordinates of the face j_3 obtained from the director vector of the reflected ray of the second reflection and from Eqs. (14) and (15):

$$\theta_{i_{j_3}} = \arccos\left(\vec{u}_r^{\,rj_2j_3} \cdot \vec{u}_{z_{j_3}}\right) \tag{51}$$

$$\phi_{i_{j_3}} = \arctan\left(\frac{\vec{u}_r^{\,rj_2j_3} \cdot \vec{u}_{y_{j_3}}}{\vec{u}_r^{\,rj_2j_3} \cdot \vec{u}_{x_{j_3}}}\right) \tag{52}$$

With $\theta_{i_{j_3}} \in [0;\pi]$ and $\phi_{i_{j_3}} \in [0;2\pi]$.

With the help of $\vec{u}_i^{j_3}$, the illuminated surface on the face j_3 is obtained by geometrical projection of the illuminated surface of the face j_2 on the face j_3. Three cases can be obtained for a given sense, they are depicted in Fig. 12 for the case of an indirect sense of triple reflection.

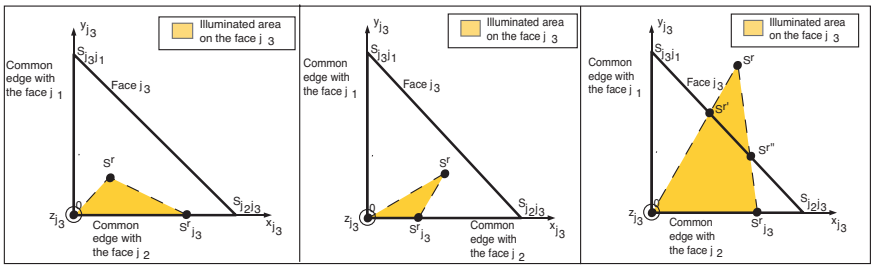

Figure 12. Illuminated surface on the face j_3 after the first and second reflection during triple reflection in the indirect sense case.

However, there are four possibilities for the observation during the third reflection occurring on j_3: shadowing effect in observation

by the face j_1 on j_3, shadowing effect in observation by the face j_2 on j_3, shadowing effect in observation by the faces j_1 and j_2 on j_3, no shadowing effect in observation. As in the single and double reflection cases, the shadowed surfaces in observation can be obtained by geometrical projection parallel to the observation direction. The three cases obtained are depicted in Fig. 13 for the case of an indirect sense of triple reflection.

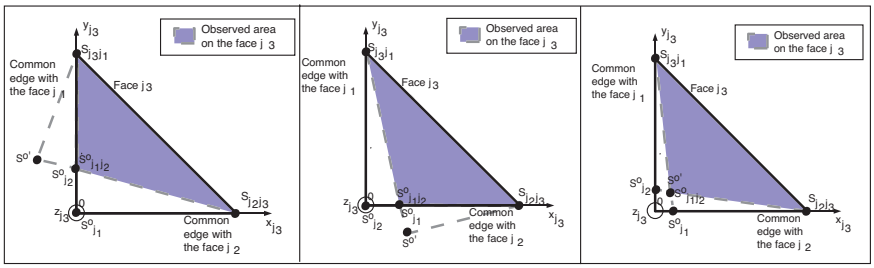

Figure 13. Shadowing effect in observation on the face j_3 for the triple reflection calculus in the indirect sense case.

Nine configurations of combination of illuminated surfaces and observed surfaces are encountered, Fig. 14 for the case of an indirect sense of triple reflection.

With the help of appropriate tests and calculus of intersection, the both illuminated and observed surface is evaluated. It can be an arbitrary triangle, an arbitrary quadrilateral or an arbitrary pentagon. These tests and calculus can be easily generalised for the two senses of triple reflection. The signature of the triple reflection $j_1 \rightarrow j_2 \rightarrow j_3$ is then derived from the signature of elementary triangle from the PO theory (appendix A) expressed in the local system of coordinates of the plate j_3. If the surface is a quadrilateral or a pentagon, it can be broken up into two or three elementary triangles, and the signature is obtained by the coherent summation of the two signatures of the elementary triangles.

The signature of the triple reflection expressed in the local system of coordinates of the plate j_3 is then evaluated in the global system of coordinates associated to the TCR k:

$$\begin{bmatrix} 0 & 0 & 0 \\ 0 & \left[S^{tr}_{j_1 j_2 j_3\ global-k}\right] & \\ 0 & & \end{bmatrix} = \left[P_{d_{j_3}}\right] \begin{bmatrix} 0 & 0 & 0 \\ 0 & \left[S^{tr}_{j_1 j_2 j_3\ local-j_3}\right] & \\ 0 & & \end{bmatrix} \times [P_{j_3 j_2}]\,[F]\ [P_{j_2 j_1}]\,[F]\ \left[P_{i_{j_1}}\right]^T \quad (53)$$

The matrix $[F]$ is obtained from Eq. (38), the matrices $[P_{dj_3}]$

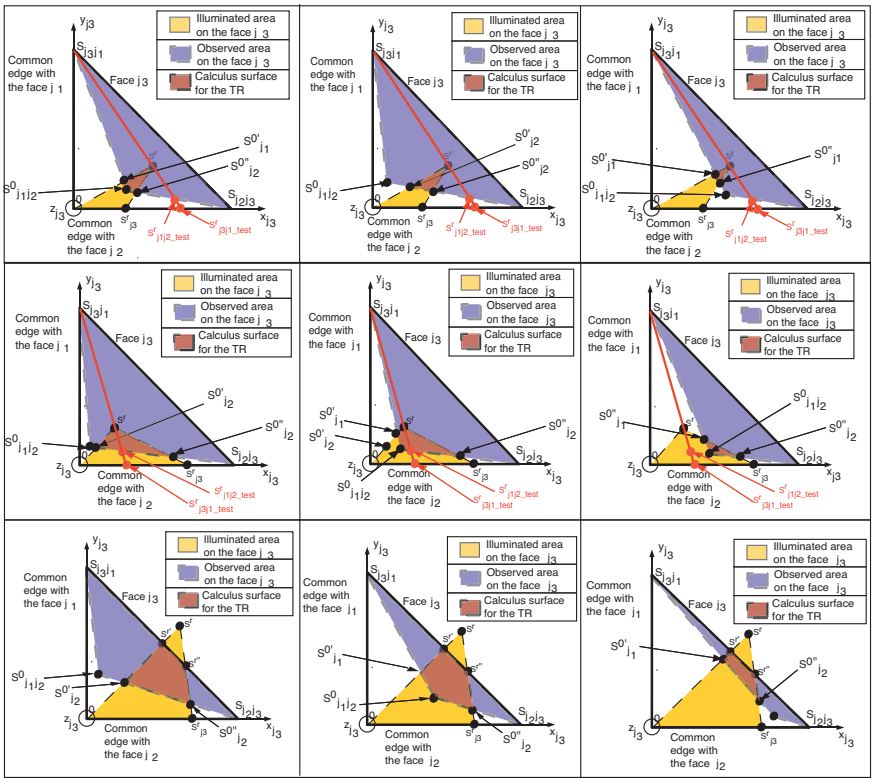

Figure 14. Intersections of illuminated and observed surfaces on the face j_3 for the triple reflection calculus in the indirect sense case.

and $[P_{ij_1}]$ are defined from Eqs. (4), (12) and (13) using appropriate subscripts. The matrices $[P_{j_2j_1}]$ and $[P_{j_3j_2}]$ are defined from Eq. (39) using appropriate subscripts.

Signature of triple reflection contribution expressed in the global system of coordinates of the trihedral reflector k is the summation of the signature of each triple reflection, that could occur, evaluated in this global system of coordinates:

$$\left[S_k^{tr}\right] = \sum_{j_1=1}^{3}\sum_{j_2=1}^{3}\sum_{j_3=1}^{3}\left[S^{tr}_{j_1j_2j_3\ global-k}\right] \quad ;\ j_1 \neq j_2 \neq j_3 \qquad (54)$$

Finally, the evaluation of the triple reflection contribution has been explained. The next section relates to the evaluation of the single diffraction contribution.

7. SINGLE DIFFRACTION OF THE TRIHEDRAL CORNER REFLECTOR

The signature of single diffraction contribution of the trihedral corner reflector k is evaluated by using the Method of Equivalent Currents (MEC) [11, 12, 14] to take into account the fringe current for the exterior edges of the TCR. These edges correspond to [AB] [BC] and [AC] as depicted in Fig. 15. The bistatic signature of the exterior edge

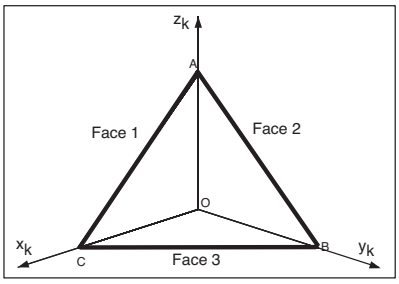

Figure 15. Exterior edges of the trihedral corner reflector.

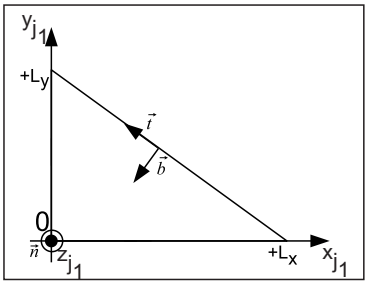

Figure 16. Exterior edge configuration.

of a face j_1, belonging to the TCR k, is evaluated in the local system of coordinates of the face j_1 from appendix B. The configuration of this exterior edge on the face j_1 is depicted in Fig. 16. So, the tangent vector, and the binomial vector of the edge are:

$$\vec{t} = -\frac{L_x}{L_{A2}}\vec{u}_{x_{j_1}} + \frac{L_y}{L_{A2}}\vec{u}_{y_{j_1}} \tag{55}$$

$$\vec{b} = -\frac{L_y}{L_{A2}}\vec{u}_{x_{j_1}} - \frac{L_x}{L_{A2}}\vec{u}_{y_{j_1}} \tag{56}$$

With

$$\vec{b} = \vec{n} \wedge \vec{t} \tag{57}$$

And

$$\vec{n} = \vec{u}_{z_{j_1}} \tag{58}$$

The length and the center of the edge are:

$$L_{A_{j_1}} = \sqrt{L_x^2 + L_y^2} \tag{59}$$

$$O_{A_{j_1}} = +\frac{L_x}{2}\vec{u}_x + \frac{L_y}{2}\vec{u}_y \tag{60}$$

So, the phase integral $I_{A_{j_1}}$ is:

$$I_{A_{j_1}} = \int_0^{L_x} e^{-jk\left(ux'+vL_y\frac{1-x'}{L_x}\right)}\,\mathrm{d}x' \tag{61}$$

And finally:

$$I_{A_{j_1}} = L_x \cdot \mathrm{sinc}\left(\frac{k(uL_x - vL_y)}{2}\right) e^{-jk\frac{uL_x+vL_y}{2}} \tag{62}$$

The ponderation term, necessary for the calculus is then:

$$P_{A_{j_1}} = L_x \cdot \mathrm{sinc}\left(\frac{k(uL_x - vL_y)}{2}\right) e^{-jk\frac{uL_x+vL_y}{2}} \cdot \frac{e^{-jkr}}{2\pi r} \tag{63}$$

Then, from the elementary signature given in the appendix B, the signature of an exterior edge of a face j_1 in a TCR k is obtained in the local system of coordinates of the face j_1. This signature is then expressed in the global system of coordinates of the TCR k with Eq. (22).

If all the three exterior edges of the TCR k are considered in the evaluation of the signature of the octahedral reflector, some edges will be taken into account many times because each edge is common to another trihedral reflector as we can see in Fig. 2. So, only the exterior edges belonging to the faces 1 and 3 of the TCRs 1 to 4 and the exterior edges belonging to the face 1 of the TCRs 5 to 8 are evaluated. The numbering of the trihedral corner reflectors and the faces in the TCR are shown in Fig. 2 and Fig. 1. So, the signature of single diffraction of the TCR k expressed in the global system of coordinates of the TCR k is:

$$\left[S_k^{sd}\right] = \begin{cases} \displaystyle\sum_{j_1=\{1,3\}} \left[S^{sd}_{j_1\ global-k}\right] & \text{if } k = \{1,2,3,4\} \\ \left[S^{sd}_{j_1\ global-k}\right]\Big|_{j_1=2} & \text{if } k = \{5,6,7,8\} \end{cases} \tag{64}$$

After evaluating all the contributions which yield the polarimetric signature of the octahedral reflector, now let us focus on the results of our calculus.

8. RESULTS

A program based on the above formulations has been developed to calculate the bistatic signature of the faceted octahedron. The Sinclair matrix is defined as:

$$[S] = \begin{bmatrix} S_{\theta\theta} & S_{\theta\phi} \\ S_{\phi\theta} & S_{\phi\phi} \end{bmatrix} \tag{65}$$

RCS data are then calculated with the following equation:

$$\sigma_{xy} = \lim_{r \to +\infty} 4\pi r^2 \left|S_{xy}\right|^2 \tag{66}$$

Where the subscripts x and y can be θ or ϕ, S_{xy} is one of the components of the Sinclair matrix of the faceted octahedron.
The internal edge length L of the octahedral reflector, shown in Fig. 2, is equal to 10λ with a frequency of 10 GHz.

Results based on our method are compared with the software FEKO [15] using a numerical method: Multi-Level Fast Multipole Method (MLFMM) which is considered as the reference. This method was used with a density of the mesh which the sampling step is $\lambda/5$ (personal computer: CPU Intel Pentium 4 at 2.4 GHz and 1 Go of RAM), this sampling step was limited due to the capacities of the computer.

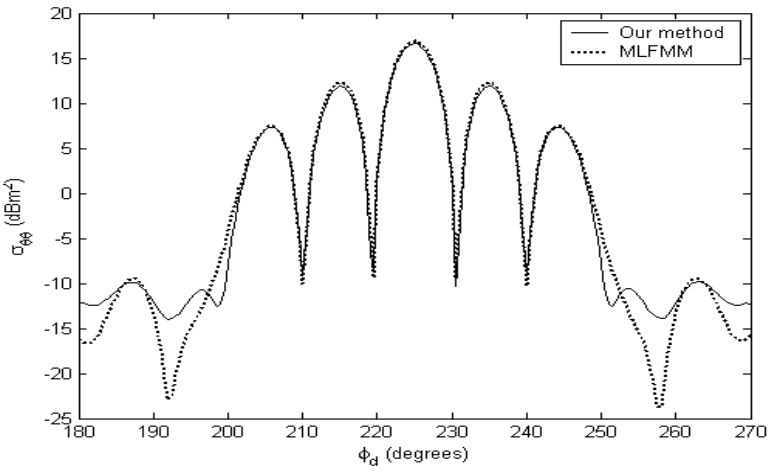

Figure 17. Bistatic RCS of the octahedral reflector in co-polarisation.

In Figs. 17 and 18, the RCS is plotted versus the observation angle ϕ_d with $\theta_d = 30°$ in the bistatic case ($\theta_i = 180 - 30° = 150°$, $\phi_i = 180 + 45° = 225°$). In Fig. 17 the RCS in co-polarisation $\sigma_{\theta\theta}$ is depicted, whereas in Fig. 18 the RCS in cross-polarisation $\sigma_{\phi\theta}$ is shown.

In Figs. 19 and 20, the RCS is plotted versus the observation angle θ_d with $\phi_d = 45°$ in the monostatic case ($\theta_i = 180° - \theta_d$, $\phi_i = 180° + \phi_d = 225°$). In Fig. 19 the RCS in co-polarisation $\sigma_{\theta\theta}$ is depicted, whereas in Fig. 20 the RCS in cross-polarisation $\sigma_{\phi\theta}$ is shown.

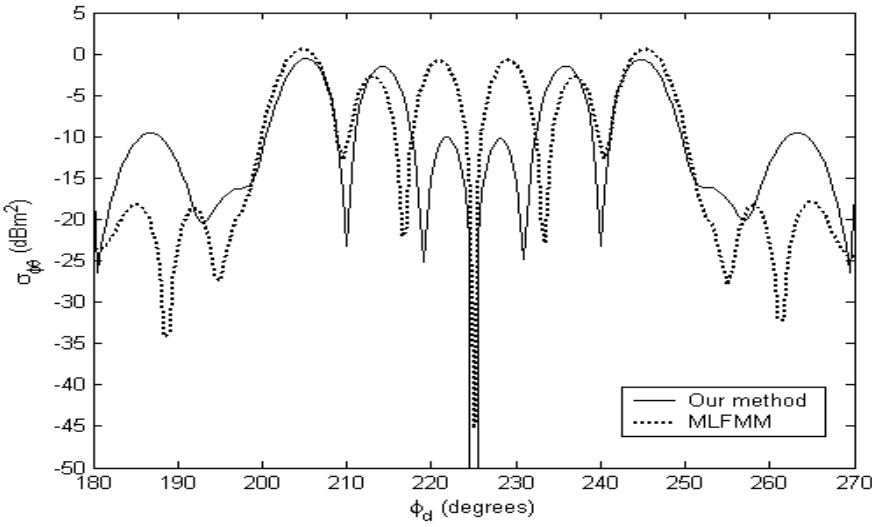

Figure 18. Bistatic RCS of the octahedral reflector in cross-polarisation.

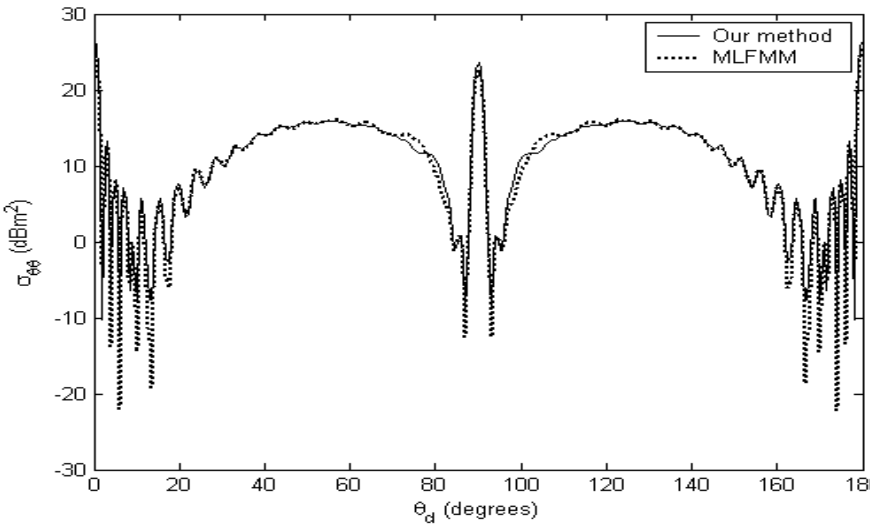

Figure 19. Monostatic RCS of the octahedral reflector in co-polarisation.

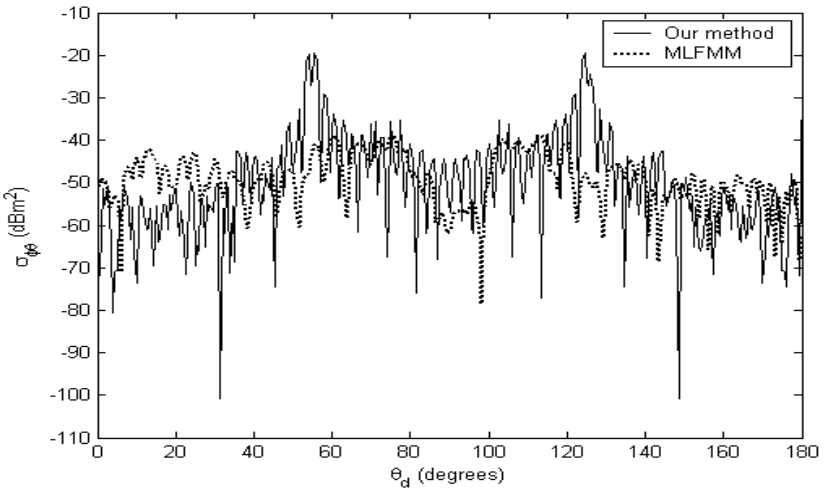

Figure 20. Monostatic RCS of the octahedral reflector in cross-polarisation.

In Fig. 19, the agreement between the two methods in co-polarisation is excellent.

From Figs. 18 and 20, for the cross-polarisation, a disagreement is observed between our method and the MLFMM. It can be attributed to that for the cross-polarisation, the results computed from the MLFMM is sensitive to the sampling step: the value used is $\lambda/5$, but also it can be due to the limit of our method. Indeed, the use of GO approximation, during double and triple reflections, assumes that the electromagnetic wave remains plane after each bounce, allowing to simplify the calculation but can alter the accuracy of the results. The PO approximation assumes that the current density is null on shadowed surfaces, neglecting for example the effect of creeping waves. The MEC is an approximation of the fringe current expression, so the concentration of the current near edges is not exactly evaluated. By studying the special case of the backscattering from isosceles triangular plates from the Geometrical Theory of Diffraction method, Ross et al. have underlined that the second-order diffraction (interaction between two edges) can contribute in the RCS for grazing angles [16]. The contributions of the second-order diffraction, the reflection-diffraction and diffraction-reflection for example, were not taken into account in our model and can affect the values of the results in the cross-polarisation. This can also explain the differences in the bistatic case, in Fig. 17, for $\phi_d \in [180°; 200°]$ and $\phi_d \in [250°; 270°]$. A prospect of

the paper is to take into account the second order diffraction from the formula of Michaeli [17].

Our calculus is fast but another advantage of our method is that each component contributing in the total signature can be evaluated separately. In Fig. 21, same variation as in Fig. 19 is shown but all the components are separated. The axis of symmetry at $\theta_d = 90°$ is

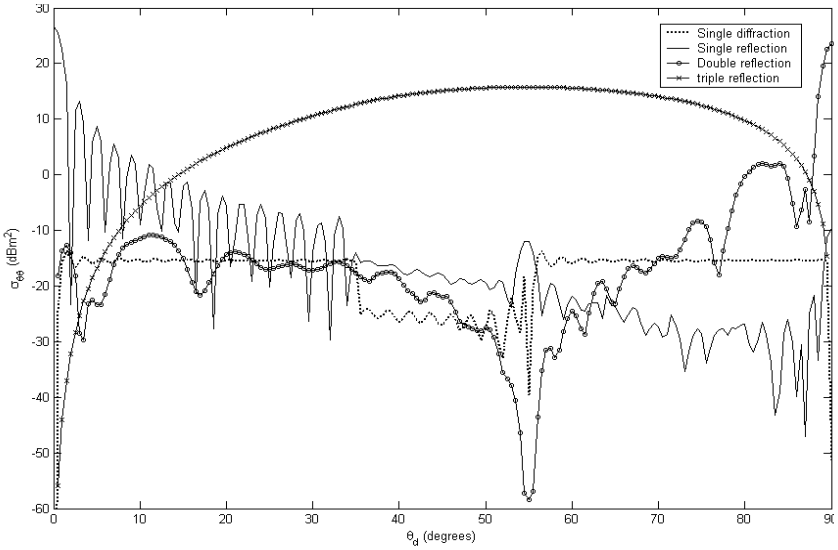

Figure 21. Components of the monostatic RCS of the octahedral reflector in co-polarisation.

observed in Fig. 19. This was expected because of the geometry of the object. For $\theta_d \in [0°; 90°]$ the incident wave illuminates mainly the TCR numbered 1 then the TCR numbered 6 for $\theta_d \in [90°; 180°]$.

The value of the single reflection contribution at 0° corresponds to the specular of the square plate composed by the four faces numbered 3 of the TCRs numbered 1 to 4. The value is $\sigma_{\theta\theta} = 26,5$ dBm^2 which verifies the value obtained with the expression: $\sigma = 4\pi \left(\frac{2L^2}{\lambda}\right)^2$.

The value obtained at 90° in the double reflection contribution is the specular of the effective rhombus composed by the faces 1 and 2 of the TCR numbered 2 and the faces 1 and 2 of the TCR numbered 6. This effective rhombus has diagonal lengths of $L/\sqrt{2}$ and $2L$. The specular value is obtained with $\sigma = 4\pi \left(\frac{2L^2}{\sqrt{2}\lambda}\right)^2$, and finally $\sigma = 23,5\,\text{dBm}^2$. This value is also verified on Fig. 21.

For $\theta_d \in [20°; 80°]$ the major contribution is due to the triple

reflection contribution created between the three faces of the TCR numbered 1.

For $\theta_d \in [0°; 35°]$, all the edges of the TCRs numbered 1 to 4 are excited. From the value $\theta_d = 35°$, the edge of the face 3 of the TCR numbered 3 is shadowed. From the value $\theta_d = 55°$, the edges of faces 1 and 2 of the TCR numbered 6 are excited. For $\theta_d = 90°$ only the edges of the TCRs 1 and 6 are illuminated. These phenomena are observed in the behaviour of the single diffraction contribution.

For $\theta_d \in [0°; 30°]$ an interference effect is shown in Fig. 19. This phenomenon is due to the interference effect obtained on the single, double and triple reflection contributions between the TCRs numbered 1 to 4. These fast variations occur in Fig. 21.

The principal advantage of our method is the requirement in CPU time. For the bistatic simulation shown in Figs. 17 and 18, the MLFMM method requires 54 minutes 34 seconds whereas only 2.4 seconds for our method to obtain the four components of the scattering matrix. For the monostatic simulation shown in Figs. 19 and 20, the MLFMM method requires 138 hours 20 minutes whereas only 5.25 seconds for our method to obtain the four components of the scattering matrix.

9. CONCLUSION

The hybridation of PO, GO and MEC is a very good approach for the evaluation of monostatic and bistatic signature of complex structure, such as octahedral reflector. The evaluation of the signature of this particular object requires the knowledge of the bistatic signature of triangularly shaped trihedral corner reflector on 4π steradians and its evaluation was completely described in this paper with the help of GO for the evaluation of shadowed surfaces. Numerical results presented in this paper show good agreement with the numerical method MLFMM for the co-polarisation and some progress may be required for the cross-polarisation. Comparatively to MLFMM, our method requires many less space and CPU time.

APPENDIX A. SIGNATURE OF AN ARBITRARY SHAPED TRIANGLE

A.1. Signature Of An Arbitrary Plane Polygonal Reflector

A plane polygonal reflector with surface S, contained in the plane $(0, x, y)$, is considered. As shown in Fig. A1, the axis $(0z)$ is the normal to the plane reflector ($\vec{n} = \vec{u}_z$). The direction vectors of the incident

and scattered rays are defined by the spherical angles (θ_i, ϕ_i) and (θ_d, ϕ_d). The incident and scattered field components are expressed, in FSA convention, in the spherical basis $(\vec{u}_r^i, \vec{u}_\theta^i, \vec{u}_\phi^i)$ and $(\vec{u}_r^d, \vec{u}_\theta^d, \vec{u}_\phi^d)$. The

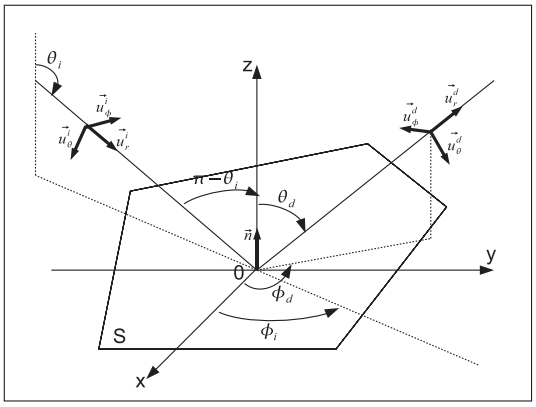

Figure A1. Configuration for the bistatic scattering by the surface of a plane polygonal reflector.

Physical Optics approximation is applied in the electric and magnetic field equations expressed in far field:

$$\vec{E}_d(\vec{r}) = -jk\frac{e^{-jkr}}{4\pi r}\iint_S \left[\left(\vec{M}(\vec{r}\,') - Z_0\vec{J}(\vec{r}\,')\wedge\vec{u}_r^d\right)\wedge\vec{u}_r^d\right] e^{+jk\vec{u}_r^d\cdot\vec{r}\,'}\,\mathrm{d}S' \tag{A1}$$

$$\vec{H}_d(\vec{r}) = jk\frac{e^{-jkr}}{4\pi r}\iint_S \left[\left(\vec{J}(\vec{r}\,') + \frac{1}{Z_0}\vec{M}(\vec{r}\,')\wedge\vec{u}_r^d\right)\wedge\vec{u}_r^d\right] e^{+jk\vec{u}_r^d\cdot\vec{r}\,'}\,\mathrm{d}S' \tag{A2}$$

Where

- $\vec{r}$ is the observation point vector ($\vec{r} = r\vec{u}_r^d$).
- $\vec{r}\,'$ is the integration point vector to the surface S of the object, directly illuminated by the incident plane wave.
- $k = 2\pi/\lambda$ is the wave number.
- $(\vec{E}_d(\vec{r}), \vec{H}_d(\vec{r}))$ is the electromagnetic field scattered at the observation point.
- $J(\vec{r}\,')$ and $M(\vec{r}\,')$ are the electric and magnetic surface current density at the integration point.

And we have:

$$\vec{u}_r^i = \begin{bmatrix} \sin(\theta_i)\cos(\phi_i) \\ \sin(\theta_i)\sin(\phi_i) \\ \cos(\theta_i) \end{bmatrix} \tag{A3}$$

$$\vec{u}_r^d = \begin{bmatrix} \sin(\theta_d)\cos(\phi_d) \\ \sin(\theta_d)\sin(\phi_d) \\ \cos(\theta_d) \end{bmatrix} \tag{A4}$$

And

$$\vec{r}' = \begin{bmatrix} x' \\ y' \\ 0 \end{bmatrix} \tag{A5}$$

With vectorial operations from the magnetic or electric field equation Eqs. (A1) and (A2), and with the help of the PO approximation (Eqs. (1) and (2)), the Sinclair matrix is:

$$[S] = P_s[\tilde{S}] \tag{A6}$$

Where $\tilde{S}$ is the elementary scattering matrix of the surface of a plane reflector with arbitrary shape:

$$[\tilde{S}] = \begin{bmatrix} \cos\theta_d\,\cos(\phi_d - \phi_i) & \cos\theta_d\,\cos\theta_i\,\sin(\phi_d - \phi_i) \\ \sin(\phi_d - \phi_i) & \cos\theta_i\,\cos(\phi_d - \phi_i) \end{bmatrix} \tag{A7}$$

P_s is a ponderation term which depends on the observation distance r, on the wavelength λ, on the incidence and observation angles and on the shape of the surface reflector:

$$P_s = j\frac{e^{-jkr}}{\lambda r}\int_y\int_x e^{-jk(ux'+vy')}\,\mathrm{d}x'\mathrm{d}y' \tag{A8}$$

Because, we can write:

$$(\vec{u}_r^i - \vec{u}_r^d)\cdot\vec{r}' = ux' + vy' \tag{A9}$$

with

$$u = \sin(\theta_i)\cos(\phi_i) - \sin(\theta_d)\cos(\phi_d) \tag{A10}$$

$$v = \sin(\theta_i)\sin(\phi_i) - \sin(\theta_d)\sin(\phi_d) \tag{A11}$$

Then, these expressions can be applied for the particular case of a right triangle.

A.2. Signature of a Right Triangle

The right triangle is shown in Fig. A2.
The calculation of P_s for this case is easily evaluated by analytical integration and is finally given by:

$$P_s = jk\frac{L_xL_y}{2}\cdot\psi\left(\frac{kuL_x}{2},\frac{kvL_y}{2}\right)\frac{e^{-jkr}}{2\pi r} \tag{A12}$$

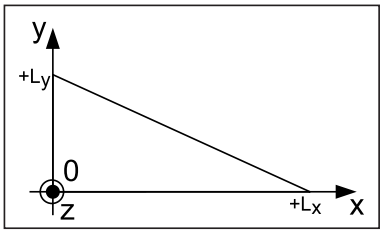

Figure A2. Configuration for the bistatic scattering by the surface of a right triangle.

With:

$$\psi(x,y) = \frac{\mathrm{sinc}(y)e^{-jy} - \mathrm{sinc}(x)e^{-jx}}{j(x-y)} \tag{A13}$$

And

$$\psi(0,0) = 1 \qquad \lim_{\substack{x \to y \\ x \neq 0}} \psi(x,y) = \frac{e^{-jx}}{x}\left[\mathrm{sinc}(x) - e^{-jx}\right] \tag{A14}$$

The bistatic signature matrix is then obtained with Eqs. (A6), (A7) and (A12).

A.3. Signature of the Arbitrary Shaped Triangle

The triangle is located by three points in a given system of coordinates. In fact, an arbitrary triangle is the union of two right triangles for which the bistatic signature in a local system of coordinates was studied in the precedent subsection.

The arbitrary shaped triangle is decomposed into two right triangles with the evaluation of an height of the arbitrary triangle as shown in Fig. A3. So, the two right triangles obtained are defined in their own local system of coordinates as shown in Fig. A3. These systems of coordinates can be evaluated using the Euler rotation with the help of the rotation angles for the first right triangle (SHP_1): $\alpha_{e_{t1}}, \beta_{e_{t1}}, \gamma_{e_{t1}}$ and for the second one (SHP_2): $\alpha_{e_{t2}}, \beta_{e_{t2}}, \gamma_{e_{t2}}$. These angles are evaluated from the coordinates of each point of the triangle. With the expressions of the systems of coordinates, spherical angles in incidence and diffraction can be known with Eqs. (14) and (15).

The signature of each triangle is then calculated in its own local system of coordinates from the signature of a right triangle, as seen in subsection A.2. The signature of each right triangle expressed in its

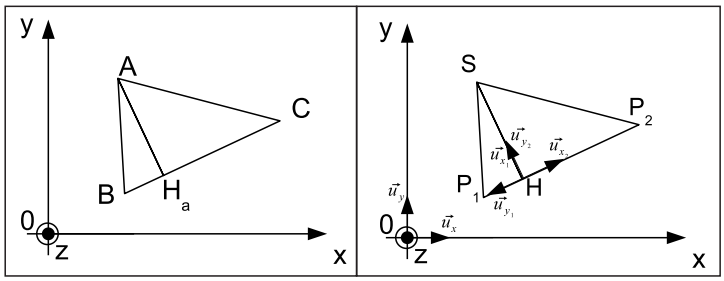

Figure A3. Decomposition of the arbitrary shaped triangle.

own local system of coordinates is then evaluated in the global system of coordinates where the arbitrary shaped triangle is defined:

$$\begin{bmatrix} 0 & 0 & 0 \\ 0 & \left[S_{t^i-global}\right] \\ 0 \end{bmatrix} = Tr \cdot \left([P_{dt^i}] \begin{bmatrix} 0 & 0 & 0 \\ 0 & \left[S_{t^i-local}\right] \\ 0 \end{bmatrix} [P_{it^i}]^T \right) \tag{A15}$$

Tr is a phase correction to include the translation of the origin.

$$Tr = e^{-jk(\vec{u}_r^i - \vec{u}_r^d)\cdot\overrightarrow{0H}} \tag{A16}$$

The matrices $[P_{dt^i}]$ and $[P_{it^i}]$ are obtained from Eqs. (4), (12) and (13).

Signature of the arbitrary shaped triangle expressed in the global system of coordinates is the summation of the signature of each right triangle evaluated in the global system of coordinates:

$$[S] = \sum_{t^i=1}^{2} \left[S_{t^i-global}\right] \tag{A17}$$

It can be noted that the bistatic signature of an arbitrary shaped triangle can be easily used to evaluate the bistatic signature of more complex polygon, by using appropriate combinations and coherent summations.

APPENDIX B. SIGNATURE OF THE DIFFRACTION BY AN EDGE

The bistatic signature of the diffraction by a metallic edge is computed by using the Method of Equivalent Currents (also named by Mitzner: Incremental Length Diffraction Coefficients) [7–10]. This method permits to describe the fringe current expression, source of the

diffracted field by edges with the help of fictive currents. The edge is assumed to be locally rectilinear around each point of the considered contour. The diffracted field is then calculated by a single integral of the equivalent currents on the contour L of the edge:

$$\vec{E}^d = jk\frac{e^{-jkr}}{4\pi r} \times \int_L \left[Z_0 I_e(\vec{r}\,')\vec{u}_r^d \wedge \left(\vec{u}_r^d \wedge \vec{t}(\vec{r}\,')\right) + I_m(\vec{r}\,')\vec{u}_r^d \wedge \vec{t}(\vec{r}\,')\right] e^{+jk\vec{u}_r^d\cdot\vec{r}\,'}\,\mathrm{d}l\,' \tag{B1}$$

Where

- $\vec{r}$ is the observation point vector ($\vec{r} = r\vec{u}_r^d$).
- $\vec{r}\,'$ is the integration point vector on the contour L of the edge of the target, directly illuminated by the incident plane wave.
- $k = 2\pi/\lambda$ is the wave number.
- $(\vec{E}_d(\vec{r}), \vec{H}_d(\vec{r}))$ is the electromagnetic field diffracted at the observation point.
- $\vec{t}(\vec{r}\,')$ is the unit tangent vector of the edge at the integration point;
- $\vec{I}_e(\vec{r}\,') = I_e(\vec{r}\,')\vec{t}$ and $\vec{I}_m(\vec{r}\,') = I_m(\vec{r}\,')\vec{t}$ are the electric and magnetic equivalent currents at the integration point;

The expressions of the electric and magnetic equivalent currents at the integration point are obtained from the theory of Mitzner or from the theory of Michaeli which were all two written on the same formalism by Knott [14]:

$$I_e(\vec{r}\,') = \frac{2j}{kZ_0}\left\{D_e\left[\vec{E}^i(\vec{r}\,')\cdot\vec{t}(\vec{r}\,')\right] + D_m\left[Z_0 H^i(\vec{r}\,')\cdot\vec{t}(\vec{r}\,')\right]\right\} \tag{B2}$$

$$\vec{I}_m(\vec{r}\,') = \frac{2j}{k}D_m\left[Z_0 H^i(\vec{r}\,')\cdot\vec{t}(\vec{r}\,')\right] \tag{B3}$$

Where $(\vec{E}^i(\vec{r}\,'), H^i(\vec{r}\,'))$ is the incident electromagnetic field at the integration point, and (D_e, D_{em}, D_m) are the coefficients of the MCE [14] which depend on local angles (β_i, ψ_i) and (β_d, ψ_d) defined in the local basis $(\vec{n}, \vec{t}, \vec{b})$ associated to the edge, as depicted in Figs. B1 and B2 for a rectilinear edge with an aperture of $(2-n)\pi$. The angles β_i and β_d are respectively defined in the incidence plane $Pi = (\vec{u}_r^i, \vec{t})$ and in the diffraction plane $Pd = (\vec{u}_r^d, \vec{t})$ with:

$$\beta_i = \arccos(\vec{u}_r^i \cdot \vec{t}) \tag{B4}$$

$$\beta_d = \arccos(\vec{u}_r^d \cdot \vec{t}) \tag{B5}$$

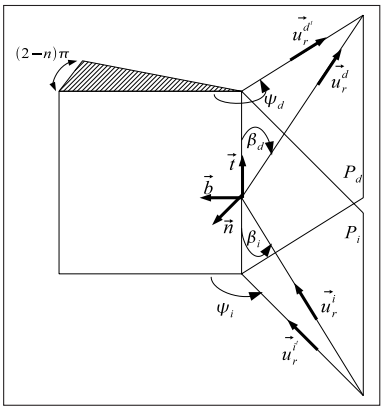

Figure B1. Definition of angles β_i and β_d in the incidence and diffraction plane.

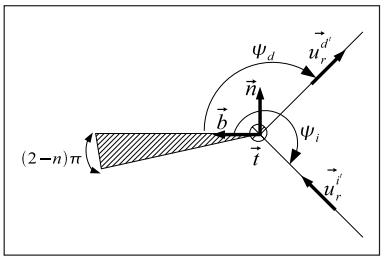

Figure B2. Definition of angles ψ_i and ψ_d in the normal plane of the edge.

The angles ψ_i and ψ_d are respectively defined in the planes $(\vec{u}_r^{i^t}, \vec{b})$ and $(\vec{u}_r^{d^t}, \vec{b})$ with:

$$\psi_i = \pi - [\pi - \arccos(-\vec{u}_r^{i^t} \cdot \vec{b})] Sign(-\vec{u}_r^{i^t} \cdot \vec{n}) \tag{B6}$$

$$\psi_d = \pi - [\pi - \arccos(-\vec{u}_r^{d^t} \cdot \vec{b})] Sign(-\vec{u}_r^{d^t} \cdot \vec{n}) \tag{B7}$$

with

$$\vec{u}_r^{i^t} = \frac{\vec{u}_r^i - (\vec{u}_r^i \cdot \vec{t})\vec{t}}{\left\| \vec{u}_r^i - (\vec{u}_r^i \cdot \vec{t})\vec{t} \right\|} \tag{B8}$$

and

$$\vec{u}_r^{d^t} = \frac{\vec{u}_r^d - (\vec{u}_r^d \cdot \vec{t})\vec{t}}{\left\| \vec{u}_r^d - (\vec{u}_r^d \cdot \vec{t})\vec{t} \right\|} \tag{B9}$$

The angles ψ_i and ψ_d must respect the condition: $\psi_i, \psi_d \in [0; n\pi]$.

The diffraction coefficients of the MEC are given for the half-plane $(n = 2)$, by the relations [14]:

$$D_e = \frac{\sin(\psi_i/2)}{\sin^2 \beta_i [\sin(\alpha/2) + \cos(\psi_i/2)]} \tag{B10}$$

$$D_{em} = \frac{-Q\cos(\psi_d)}{2\sin^2 \beta_i \sin(\alpha/2)[\sin(\alpha/2) + \cos(\psi_i/2)]} - \frac{\cos(\beta_i)}{\sin^2(\beta_i)} \tag{B11}$$

$$D_m = \frac{-\sin(\psi_d)}{2\sin\beta_i \sin\beta_d \sin(\alpha/2)[\sin(\alpha/2) + \cos(\psi_i/2)]} \tag{B12}$$

With

$$Q = \frac{(1 + \cos\beta_d \cos\beta_i)(\cos\beta_i - \cos\beta_d)}{\sin\beta_d \sin\beta_i} \tag{B13}$$

$$\alpha = \begin{cases} -j\log(\mu + \sqrt{\mu^2 - 1}) & \text{if } \mu > 1 \\ -j\log(\mu + j\left|\sqrt{1-\mu^2}\right|) & \text{if } |\mu| \leq 1 \\ -j\log(\mu - \left|\sqrt{\mu^2 - 1}\right|) & \text{if } \mu < -1 \end{cases} \tag{B14}$$

With the function $\log(z) = \ln(|z|) + j\arg(z)$ and $\arg(z) \in [-\pi; \pi]$. And

$$\mu = \frac{\sin\beta_d \sin\beta_i \cos\psi_d + \cos\beta_d \cos\beta_i - \cos^2\beta_i}{\sin^2\beta_i} \tag{B15}$$

So, the coefficients of the MEC can be computed and used to calculate the signature by the edge of a polygonal plane. Indeed, with vectorial operations from Eqs. (B1), (B2) and (B3), and with the help of geometrical properties of the problem, shown in Fig. B3, the sinclair matrix can be obtained:

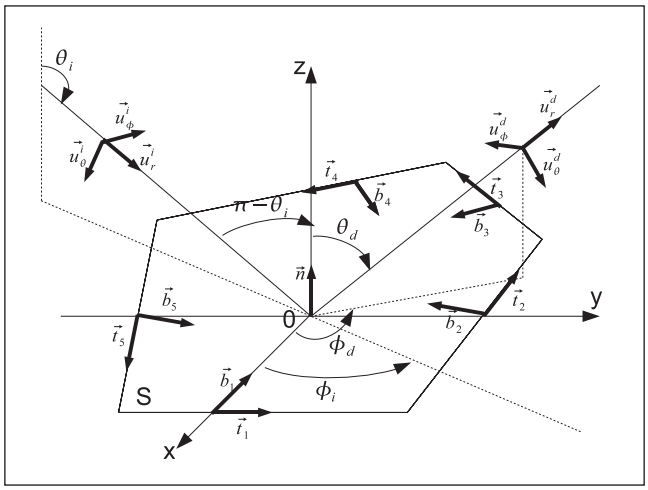

Figure B3. Configuration for the diffraction by edges of a plane polygonal reflector.

$$[S^A] = P_A[\tilde{S}^A] \tag{B16}$$

Where P_A is a ponderation term which depends on the observation distance r, the wavelength λ, the incidence and observation angles and

on the length of the edge:

$$P_A = I_A \frac{e^{-jkr}}{2\pi r} \tag{B17}$$

with

$$I_A = \int_L e^{-jk(\vec{u}_r^i - \vec{u}_r^d)\cdot\vec{r}'} \, \mathrm{d}l' \tag{B18}$$

And $\tilde{S}^A$ is the elemental diffraction matrix of the edge of the plane polygonal reflector:

$$\begin{aligned}
\tilde{S}^A_{\theta\theta} = & -\cos\theta_d(t_x\cos\phi_d + t_y\sin\phi_d)\{D_e\cos\theta_i(t_x\cos\phi_i + t_y\sin\phi_i) \\
& -D_{em}(t_x\sin\phi_i - t_y\cos\phi_i)\} \\
& +(t_x\sin\phi_d - t_y\cos\phi_d)D_m(t_x\sin\phi_i - t_y\cos\phi_i) \qquad \text{(B19)} \\
\tilde{S}^A_{\theta\phi} = & +\cos\theta_d(t_x\cos\phi_d + t_y\sin\phi_d)\{D_e(t_x\sin\phi_i - t_y\cos\phi_i) \\
& +D_{em}\cos\theta_i(t_x\cos\phi_i + t_y\sin\phi_i)\} \\
& +(t_x\sin\phi_d - t_y\cos\phi_d)D_m\cos\theta_i(t_x\cos\phi_i + t_y\sin\phi_i) \qquad \text{(B20)} \\
\tilde{S}^A_{\phi\theta} = & (t_x\sin\phi_d - t_y\cos\phi_d)\{D_e\cos\theta_i(t_x\cos\phi_i + t_y\sin\phi_i) \\
& -D_{em}(t_x\sin\phi_i - t_y\cos\phi_i)\} \\
& +\cos\theta_d(t_x\cos\phi_d + t_y\sin\phi_d)D_m(t_x\sin\phi_i - t_y\cos\phi_i) \qquad \text{(B21)} \\
\tilde{S}^A_{\phi\phi} = & -(t_x\sin\phi_d - t_y\cos\phi_d)\{D_e(t_x\sin\phi_i - t_y\cos\phi_i) \\
& +D_{em}\cos\theta_i(t_x\cos\phi_i + t_y\sin\phi_i)\} \\
& +\cos\theta_d(t_x\cos\phi_d + t_y\sin\phi_d)D_m\cos\theta_i(t_x\cos\phi_i + t_y\sin\phi_i) \qquad \text{(B22)}
\end{aligned}$$

Finally, let us observe that the bistatic signature of the diffraction by a metallic edge is evaluated for any incidence and observation angles with the help of an elemental diffraction matrix which can describe the diffraction phenomenon, and with the help of a ponderation term which applies the geometry of the problem.

REFERENCES

1. Bradley, C. J., P. J. Collins, J. Fortuny-Guasch, M. L. Hastriter, G. Nesti, A. J. Terzuoli, Jr. and K. S. Wilson, "An investigation of bistatic calibration objects," *IEEE Trans. Geos. Rem. Sens.*, Vol. 43, No. 10, 2177–2184, 2005.
2. Lo, Y. C. and B. K. Chung "Polarimetric RCS calibration using reference reflectors," *J. Electromagn. Waves and Applicat.*, Vol. 19, No. 13, 1749–1759, 2005.

3. Van Zyl, J. J., "Calibration of polarimetric radar images using only image parameters and trihedral corner reflectors responses," *IEEE Trans. Geos. Rem. Sens.*, Vol. 28, No. 3, 337–348, 1990.
4. Corona, P., G. Ferrara, C. Gennarelli, and G. Riccio, "A physical optics solution for the backscattering by triangularly shaped trihedral corners," *Ann. Télécom.*, Nos. 5–6, 557–562, 1995.
5. Polycarpou, A. C., C. A. Balanis, and C. R. Birtcher, "Radar cross section of trihedral corner reflectors using PO and MEC," *Ann. Télécom.*, Nos. 5–6, 510–516, 1995.
6. Sinclair, G., "The transmission and reception of elliptically polarized waves," *Proc. IRE*, Vol. 38, 148–151, 1950.
7. Germond, A-L., E. Pottier, and J. Saillard, "Bistatic radar polarimetry theory," *Ultra-Wideband Radar Technology*, James D. Taylor (ed.), 379–414 , CRC Press, 2000.
8. Kubické, G., C. Bourlier, and J. Saillard, "A physical optics solution for bistatic RCS of triangularly shaped trihedral corners for any incidence and observation angles," *EUCAP Conference*, Nice, November 6–10, 2006.
9. Pan, X. M. and X. Q. Sheng, "A highly efficient parallel approach of multi-level fast multipole algorithm," *J. Electromagn. Waves and Applicat.*, Vol. 20, No. 8, 1081–1092, 2006.
10. Van Tonder, J. J. and U. Jakobus, "Fast multipole solution of metallic and dielectric scattering problems in FEKO," *IEEE/ACES International Conference on Wireless Communications and Applied Computational Electromagnetics*, Honolulu, USA, April 3–7, 2005.
11. Michaeli, A., "Equivalent edge currents of arbitrary aspects of observation," *IEEE Trans. Ant. Prop.*, Vol. 32, No. 3, 252–258, 1984.
12. Michaeli, A., "Elimination of infinities in equivalent edge currents, Parts I: Fringe currents," *IEEE Trans. Ant. Prop.*, Vol. 34, No. 7, 912–918, 1986.
13. Mitzner, K. M., "Incremental length diffraction coefficients," Tech. Rep. No. AFAL-TR-73-296, Aircraft Division, Northrop Corp., 1974.
14. Knott, E. F., "The relationship between Mitzner's ILDC and Michaeli's equivalent currents," *IEEE Trans. Ant. Prop.*, Vol. 33, No. 1, 112–114, 1985.
15. FEKO - EM Software and Systems, *www.feko.info*, Technopark-Stellenbosch, South Africa.

16. Ross, R. A. and M. Hamid "Backscattering from isosceles triangular metallic plates," *J. Electromagn. Waves and Applicat.*, Vol. 19, No. 13, 1177–1786, 2005.
17. Michaeli, A., "Equivalent currents for second-order diffraction by the edges of perfectly conducting polygonal surfaces," *IEEE Trans. Ant. Prop.*, Vol. 35, No. 2, 183–190, 1987.